Diffractive Interference Design Using Front and Rear Surface Metal and Dielectric Nanoparticle Arrays for Photocurrent Enhancement in Thin Crystalline Silicon Solar Cells

Enrico Massa,*,[†] Vincenzo Giannini,[†] Nicholas P. Hylton,[†] N. J. Ekins-Daukes,[†] Samarth Jain,[‡] Ounsi El Daif,[§,⊥] and Stefan A. Maier[†]

[†]Blackett Laboratory, Department of Physics, Imperial College London, London SW7 2AZ, U.K.
[‡]Silhouette Rainbows, Sikandra, Agra, India
[§]IMEC, Kapeldreef 75, B-3001 Heverlee, Belgium

ABSTRACT: Using an interference design model we were able to quickly optimize the nanophotonic control afforded by metal and dielectric nanoparticle arrays to enhance the absorption and photocurrent in a thin crystalline silicon solar cell, which were simulated via full field electromagnetic FEM calculations. Fabry−Perot interference fringes introduced by placing structures on the front and rear surfaces are shown to lead to significant enhanced light trapping in the absorbing silicon layer. We report a 46.7% increase in the estimated short-circuit photocurrent over the solar spectrum (AM 1.5G)

range of 300−1100 nm for a 1 μm thick crystalline silicon solar cell with metal and dielectric nanoparticle arrays designed using interference modeling. The enhancement was achieved by placing nanoparticle arrays on the front and rear surface of the cell, where the particles on the front surface are dielectric (Si) and those on the rear surface are metal (Al). Additionally, an estimated photocurrent enhancement of 29.4% was obtained with just the aluminum nanoparticle array on the rear surface of the cell. Our study of nanoparticle arrays of metal (aluminum) and dielectrics (silicon, titanium oxide, aluminum oxide, and silicon nitride) involved different radius, pitch, and position on the front and rear surface of silicon solar cells with antireflection coatings. Improved light trapping and absorption thanks to the arrays are unambiguously shown. The rear surface array is shown to broadly reduce the reflectance of the cell via multiple Fabry−Perot resonances due to the interference of the incident and diffracted field from the array of particles. The front surface array broadly reduces the reflectance due to the excitation of local resonances and preferential scattering into the substrate. Together with local resonance excitation, these two combined effects are significant for the design of thin-film solar cells with light-trapping properties to increase the absorption and improve cell performance.

KEYWORDS: thin-film, silicon, solar cells, nanoparticle, interference, photocurrent enhancement
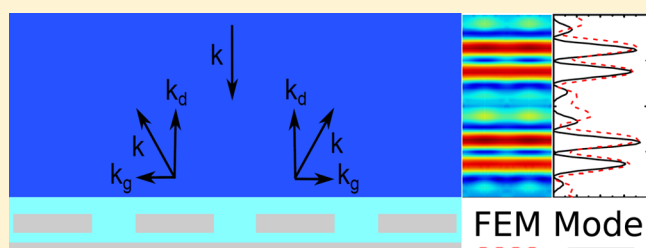
Photovoltaic (PV) power generation has the potential to meet increased energy demand from renewable sources and has displayed remarkable growth in recent years.[1,2] Despite this expansion, a reduction of investment costs on PV systems is still required to be competitive compared to other energy sources. Currently, the majority of the solar cells are based on silicon wafers with a thickness between 180 and 300 μm in order to fully absorb the entire solar spectrum, and a significant part of their cost is due to the fabrication and processing of the semiconductor itself.[3] One approach to reduce costs is to use thin-film crystalline solar cells, with film thicknesses in the range of 1−2 μm, which use much less semiconductor material. However, a thin-film solar cell is optically thin, so it shows decreased absorption, especially in the 600−1100 nm spectral range of the solar spectrum. Methods for increasing the optical depth (hence the absorption) in thin crystalline silicon materials therefore represent an attractive prospect for improving the cost efficiency of solar energy production.[4−7]

Because of their strong interaction with light,[8−13] metal and dielectric nanoparticle arrays[14−16] have recently been studied in order to improve antireflection and absorption properties of standard and thin-film solar cells.[17−20] The understanding is that scattering from the nanoparticles can increase the effective optical path length in the cell and enhance its light-trapping properties.[21] In fact, angular randomization of the scattered light can increase light absorption in an optical medium up to a factor of $4n^2$, where n is the refractive index of the medium,[4,5] which is obtained via micrometer-sized[22] or nanosized[23−27] texturing of the solar cells. Particles on the front surface of the substrate have also been shown to exhibit local resonances that preferentially scatter in the substrate, decreasing the reflectivity.[18,19] Indeed, diffraction from nanoparticle arrays,[28] and not just scattering from single particles, can play a significant role in

providing enhanced light absorption by creating a standing wave due to the interference between the incident and diffracted waves in the vertical direction. The standing wave pattern produces regions with high field concentration due to the interference of waves with different k-vectors along the direction of the incident field, which can be used to further increase the scattering from nanoparticles, albeit at the cost of higher losses.[29] Since using metal nanoparticles results in significantly higher scattering at the expense of higher parasitic losses compared to dielectrics, a physical understanding of parasitic losses is required in order to control and minimize them.[30,31] In our view, to maximize the absorption, the objective is to obtain a standing wave that peaks inside the silicon absorber and that interferes destructively in the absorbing nanoparticles in order to reduce losses. In this paper we compare the benefit of using metal and dielectric nanoparticles in different positions of the solar cell, comparing the effect of interference and diffraction on the field profile inside a thin film, and explain how to obtain the best absorption enhancement for a thin-film absorber.

We have first modeled a cell with nanoparticle arrays using a simple model of the interference between the incident and diffracted waves, for the case of strong diffraction. Our simple model was also used to select a range for the geometrical parameters of the cell, which was modeled via full field electromagnetic simulations. Remarkably, using this simple model, we were able to predict and explain the standing wave pattern inside the silicon layer caused by diffraction from arrays of nanoparticles placed on the rear surface of the cell. We show that having an array of particles on the rear surface of the cell broadly reduces the reflectance from the cell and increases the absorption in the silicon due to diffracted modes that strongly modify the standard Fabry−Perot resonances of the cell, creating standing waves with high field localization. The front surface array broadly reduces the reflectance due to the excitation of local resonances and preferential coupling into the substrate. This result is significant for the design of thin-film solar cells with light-trapping properties to increase absorption.

■ DIFFRACTIVE INTERFERENCE MODEL

Our model considers the interference along the thickness of the cell between the incident plane wave of wave-vector k and the wave diffracted by the array of wave-vector k_d, shown in Figure 1. The structure considered consists of a 1 μm thick silicon cell
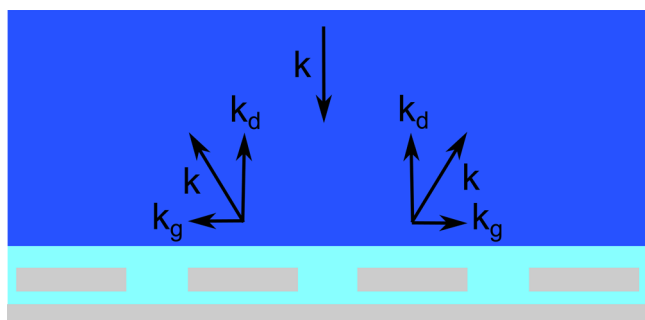

Figure 1. Wave-vector of the incident and diffracted light by the rear surface nanoparticle array. The vertical component of the wave-vector of the diffracted light, $k_d = (k^2 - k_g^2)^{1/2}$, is different from the incident wave-vector k. Fabry−Perot fringes are caused by the interference along the vertical direction of these two waves with different wave-vectors.

with a silica antireflection (AR) coating and different nanoparticle arrays placed on the rear surface of the cell.

Because of diffraction from the grating of periodicity (pitch) L, the wave-vector of the vertical component of the diffracted light in the first order can be written as $k_d = (k^2 - k_g^2)^{1/2}$, where $k_g = 2\pi/L$ is the wave-vector of the grating, which is horizontal and can have a positive or negative sign. Due to the metal reflection, the diffracted wave has an additional phase compared to the incident wave, which can be approximated by π as for a perfect reflector. The total electric field in the upper part of the cell can therefore be expressed as

$$E_{tot} = E_0 e^{ikz} + E_r e^{-ikz} + E_d e^{-ik_d z} \tag{1}$$

where E_0 is the incident field, E_r is the reflected field, E_d is the diffracted field, and a global arbitrary phase can be introduced that has the effect of shifting the standing wave along the z direction. The electric field intensity can be calculated by taking the square of the real part of eq 1, which can be averaged along the z direction for a specified finite thickness of the absorbing layer (1 μm in our case). Since the reflected field has the same k-vector as the incident field, it interferes with the incident wave without generating a variation in amplitude. In fact, changing the ratio between E_d and E_r, i.e., the amount of light diffracted versus that reflected, does not modify the interference pattern but only scales the total intensity. Therefore, the effect of changing the size of the nanoparticles, in this approximation, is only to change the ratio of E_d to E_r. By changing the wavelength of the incident wave and therefore the incident k-vector, it is possible to obtain the electric field intensity (and therefore the absorption) in the absorbing layer of the cell and study the interference condition caused by diffraction. The interference between the incident and the diffracted wave, which have a different vertical wave-vector component, causes a standing wave inside the silicon absorbing layer of the cell. The aim of the optimization procedure, which can be carried out for a specific target wavelength or for the entire solar spectrum, is to obtain a standing wave with a high average field inside the absorbing layer (i.e., with several high peaks) by changing the geometrical parameters of the array and/or the cell. It is worth noting that our model takes into account just the silicon absorbing layer to study the interference condition, but it could be extended to the full cell using the transfer-matrix method.

Via our interference model we have studied the interference condition varying the pitch of structure and the amount of light diffracted, giving a useful range of geometrical parameters for the cell to input into the more precise (and computationally demanding) full field electromagnetic simulations via the finite element method (FEM).

The FEM simulations consider only the optical properties of the cell. Taking into account also the electrical properties was shown to give very similar results when using semiconductor materials with large diffusion lengths, such as crystalline silicon.[32,33] The solar cell, without nanoparticles, is composed from the front to the rear surface by the following layers: vacuum, 120 nm of silica AR coating, 1 μm of silicon, 130 nm of silica, and an aluminum back-reflector. The incident light is coming from the top at normal incidence, as shown schematically in Figure 2a.

The nanoparticle arrays were positioned in a series of different configurations in the system, i.e., on the front surface of the silica AR layer, embedded in it 10 nm above the silicon layer, or embedded in the rear silica layer at 10 nm below the silicon layer, before the aluminum back-reflector, as shown
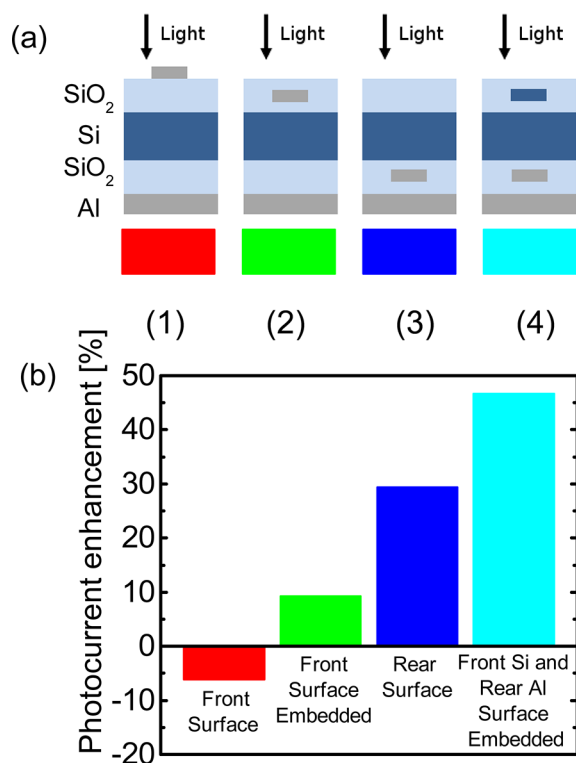
Figure 2. (a) Schematic of the positions considered for the nanoparticle arrays: front surface aluminum particles (red (1), pitch 250 nm, radius 40 nm), front surface embedded aluminum particles (green (2), pitch 250 nm, radius 80 nm), rear surface aluminum particles (blue (3), pitch 250 nm, radius 80 nm), front surface embedded silicon particles and rear surface aluminum particles (cyan (4), pitch 250 nm, radius 80 nm). (b) Estimated photocurrent enhancement calculated using eq 2 from the absorption in the silicon layer, compared to a cell without nanoparticles, for cells with nanoparticle arrays in different positions. The calculated photocurrent for each configuration is normalized to that of the cell without nanoparticles and integrated across the entire range of wavelengths from 300 to 1100 nm using the AM 1.5G solar spectrum, considering only the absorption in the silicon layer. The results shown are the best obtained for that particular position of the particles, varying pitch of the array, and the radius of the particles.

schematically in Figure 2a. The nanoparticle arrays are composed of cylinders of height h = 40 nm, with a varying radius R and pitch, of either metal (aluminum) or dielectric (silicon, titanium oxide, aluminum oxide, and silicon nitride). Cylindrical particles were chosen due to their relative ease of fabrication and since they have been shown to have better scattering properties above a substrate compared to spheres.[34] Aluminum (Al) particles[17,20,35−37] and titanium oxide (TiOx)[19] particles have been previously shown to reduce the reflectivity and enhance absorption compared to standard AR coatings. Aluminum is preferred compared to other metals due to its blue-shifted plasmon resonance, which decreases parasitic absorption in the main part of the solar spectrum. Silicon (Si), titanium oxide (TiOx), aluminum oxide (AlOx), and silicon nitride (SiNx) have been used to compare different dielectrics, which have lower absorption compared to metals. For our calculations we have used the optical constants from Palik.[38] Due to the symmetry of the structure and thanks to the periodicity, each simulation involved just one-quarter of the unit cell.

As shown schematically in Figure 2a, we have considered the case of particles placed only on the front silica antireflection coating (1), embedded in the front silica antireflection coating (2), only on the rear surface of the cell, i.e., embedded in the silica layer below the silicon layer and above the aluminum reflector (3), and with nanoparticle arrays on the front and rear surface in the two different configurations (embedded or not) (4). When having two particle arrays, i.e., on the front and rear surface, we have also considered the cases of having an array of dielectric particles embedded in the antireflection coating on the front surface, while the particles at the rear surface were made from aluminum. As a reference we have used the case of the cell without particles. We have monitored the reflectance of the cell and the absorption in the silicon layer and in the nanoparticles.

Compared to the reference cell with no nanoparticles, which has an optimized quarter-wave silica AR coating, we show that having nanoparticles on the front and rear surface with front surface embedded Si particles and rear surface Al particles significantly increases the integrated optical absorption in the silicon layer, over the useful solar spectrum (AM 1.5G), producing an estimated short-circuit photocurrent enhancement of 46.7%. An estimated photocurrent enhancement of 29.4% is obtained with just the aluminum nanoparticle array on the rear of the cell.

RESULTS AND DISCUSSION

In our full field simulations we have considered nanoparticle arrays with different pitches (150, 200, and 250 nm), composed by cylindrical nanoparticles of different radii (40, 50, 60, 70, and 80 nm) and materials (Al, Si, TiOx, AlOx, and SiNx). The arrays of nanoparticles have been placed in different positions of the cell (front surface, front surface embedded, rear surface), considering the two available combinations (front and rear surface, front surface embedded, and rear surface) when having one array on the front surface and one on the rear surface with the same particle radius, for the same pitch. As a reference we have taken the case of the cell without nanoparticles.

For the case of two metal particles, we have carried out simulations considering different particle radii independently for each array (front and rear surface), for the same pitch. In general, strong scattering at the front surface is to be avoided, since it can cause spectrum losses. Because of that, it is better to have smaller nanoparticles on the front surface or dielectric particles (which have a smaller cross section) for reduced reflectance and losses.

From the simulations we have obtained the absorption in the silicon layer of the cell and in the nanoparticle arrays and the reflectance as a function of the incident wavelength. The absorption in the silicon layer was weighted with the solar spectrum to calculate an upper limit for the short-circuit current density J_{sc}. The short-circuit current density is calculated using the following formula:

$$J_{sc} = \frac{q_e}{hc} \int_{\lambda_{min}}^{\lambda_{max}} \lambda CE(\lambda)\, A(\lambda)\, S(\lambda)\, d\lambda \qquad (2)$$

where q_e is the elementary charge, λ is the wavelength, λ_{min} and λ_{max} define the range of wavelengths considered (300 to 1100 nm in our case), h is the Planck constant, c is the speed of light, $CE(\lambda)$ is the collection efficiency, which is assumed constant and equal to 1 in the active crystalline silicon layer, $S(\lambda)$ is the solar spectrum AM 1.5G, and $A(\lambda)$ is the absorption in the

silicon layer. This method for calculating J_{sc} uses the assumption that CE = 1 and is therefore the maximum achievable. Hence in the following, it will be taken as a figure of merit to assess the effect of having arrays of nanoparticles in the solar cell. Using this method a value of 12.98 mA/cm^2 was obtained for the short-circuit current density of the reference cell, i.e., the cell without nanoparticles.

Figure 2b shows the estimated photocurrent enhancement calculated using eq 2 from the absorption in the silicon layer, compared to a cell without nanoparticles, for cells with nanoparticle arrays in different positions. The positions considered are front surface aluminum particles (red (1), J_{sc} = 12.17 mA/cm^2), front surface embedded aluminum particles (green (2), J_{sc} = 14.18 mA/cm^2), rear surface aluminum particles (blue (3), J_{sc} = 16.80 mA/cm^2), and front surface embedded silicon particles and rear surface aluminum particles (cyan (4), J_{sc} = 19.05 mA/cm^2). The calculated photocurrent for each configuration is normalized to that of the cell without nanoparticles and integrated across the entire range of wavelengths from 300 to 1100 nm using the AM 1.5G solar spectrum, considering only the absorption in the silicon layer. The results shown in Figure 2b are the best obtained for that particular position of the particles, having considered a range of particle radii and pitch.

The wavelength-dependent spectra in Figure 3 show the absorption spectra (Si_{abs}) in the silicon layer, reflectance spectra (R), and particle absorption spectra (P_{abs}) for the cases shown in Figure 2, for cells with nanoparticle arrays in different positions. For thin-film solar cells, Fabry−Perot fringes appear due to the interference of the incident and reflected waves and are the cause of the modulation in the reflectance and absorption spectra. Compared to the reference, the spectrum with the front surface aluminum particles (1) shows a slight reduction in the absorption in the silicon layer due to parasitic absorption in the particle below 400 nm, while the reflectance above that is almost unchanged. The case with the front surface embedded aluminum particles (2) shows a significant reduction in the reflectance due to stronger Fabry−Perot resonances arising from the interference between the incident and diffracted waves, but the additional light is mostly absorbed by the array of nanoparticles. The case with the rear surface aluminum particles (3) shows a further reduction in the reflectance, mostly in the range between 500 and 1000 nm, the appearance of additional Fabry−Perot peaks in the absorption and reflectance spectra, and a significant increase in the light absorbed in the silicon layer. The best result is obtained for the case with front surface embedded silicon particles and rear surface aluminum particles (4), which shows a further reduction in the reflectance in the range between 300 and 500 nm with some additional absorption in the particles limited to the 300 and 400 nm range. It is worth noting that, while bulk silicon is a broadband absorber, the silicon nanoparticles embedded on the front surface show most of the absorption between 300 and 400 nm due to the large imaginary part of Si at these wavelengths and to their size, similar to the excitation of exciton polaritons in thin crystalline Si films,[39] while the aluminum nanoparticles below the silicon layer broadly absorb above 500 nm due to the Fabry−Perot resonances.

For thin-film cells, Fabry−Perot fringes appear, as in the reference, due to the interference between the incident and reflected light from the rear reflector. With our interference model we have modeled the standing wave pattern inside the silicon layer caused by the interference between the incident
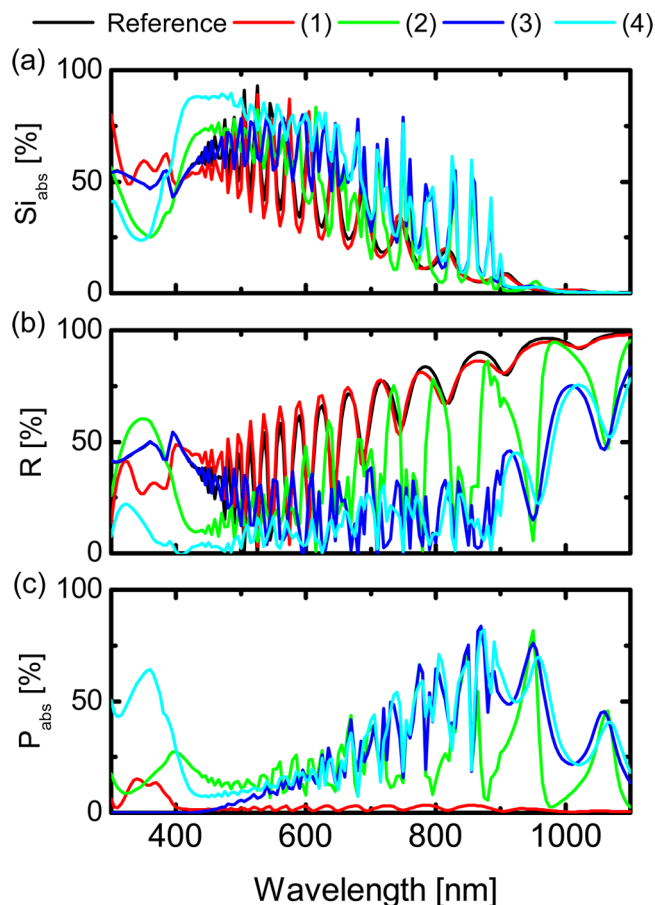

Figure 3. (a) Absorption spectra (Si_{abs}) in the silicon layer, (b) reflectance spectra (R), and (c) particle absorption spectra (P_{abs}) for the cases shown in Figure 2, for cells with nanoparticle arrays in different positions. The positions considered are front surface aluminum particles (red (1), pitch 250 nm, radius 40 nm), front surface embedded aluminum particles (green (2), pitch 250 nm, radius 80 nm), rear surface aluminum particles (blue (3), pitch 250 nm, radius 80 nm), and front surface embedded silicon particles and rear surface aluminum particles (cyan (4), pitch 250 nm, radius 80 nm). The reference cell without nanoparticle arrays is shown by the black line. The particle absorption spectrum is the sum of the absorption on the front and rear particles. The percentages are calculated from the total incident light intensity.

and the diffracted light from the aluminum nanoparticle array on the rear surface of the cell. Figure 4 shows the electric field intensity inside the cell, normalized to the incident field, at different wavelengths and the corresponding predicted interference pattern. As explained, the interference between the incident and diffracted wave with different wave vectors in the vertical direction is the cause of the electric field intensity patterns.

The peaks in the absorption in the silicon layer are obtained when the average electric field intensity inside the silicon layer is highest, and, at that condition, the field profile shows more high peaks than at a minimum. Moreover, at the maximum in the absorption, the standing wave is fully contained inside the silicon layer with a node at the interfaces, whereas the minima are obtained when peaks appear at the interfaces. As an example, Figure 4 shows a color map for the electric field at a maximum (λ = 750 nm) and a minimum (λ = 775 nm) in the silicon layer absorption, with the corresponding calculated interference pattern using our interference model. An example
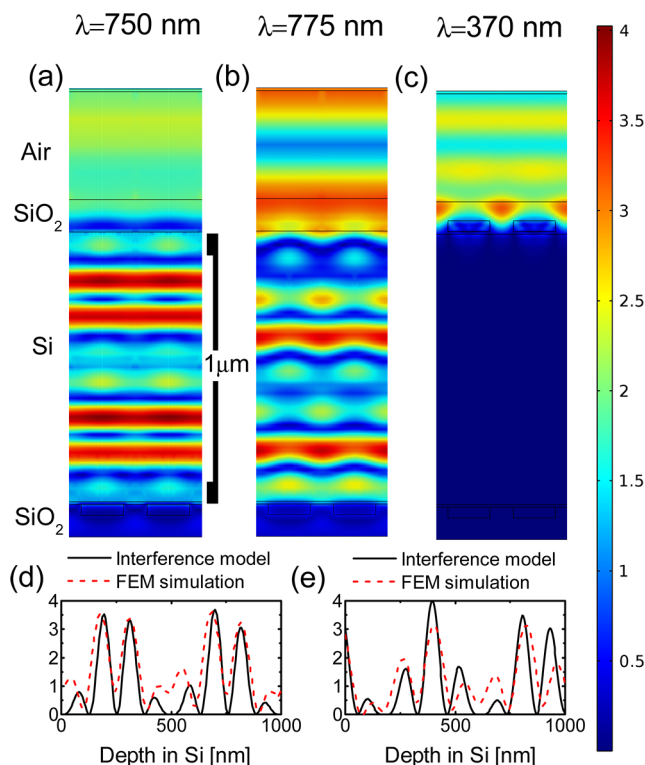
Figure 4. (a) Color map of the electric field intensity, normalized to the incident field, inside the solar cell with rear surface aluminum particles (pitch 250 nm, radius 80 nm) for the wavelength $\lambda = 750$ nm, representing a maximum in the absorption into the silicon layer, and the corresponding (d) interference pattern inside the silicon layer predicted by the interference model and the corresponding value obtained from FEM simulation, averaged along the $x-y$ directions in the cell. (b) Color map of the electric field intensity, normalized to the incident field, inside the solar cell with rear surface aluminum particles (pitch 250 nm, radius 80 nm) for the wavelength $\lambda = 775$ nm, representing a minimum in the absorption into the silicon layer, and the corresponding (e) interference pattern inside the silicon layer predicted by the interference model and the corresponding value obtained from FEM simulation, averaged along the $x-y$ directions in the cell. (c) Color map of the electric field intensity, normalized to the incident field, inside the solar cell with front surface embedded silicon particles and rear surface aluminum particles (pitch 250 nm, radius 80 nm) for the wavelength $\lambda = 370$ nm.

of the modes that are sustained by the front surface embedded silicon nanoparticles are also shown for the wavelength $\lambda = 370$ nm. The field localization around the particles and the scattering into the silicon layer are visible. The interference model predicts very well the standing wave pattern inside the silicon layer at the maximum and minimum in the silicon absorption, which can enable a quick optimization of the pitch of the array and thickness of the silicon layer.

In order to clearly demonstrate the effect of the interference due to diffraction, the wavelength-dependent spectra in Figure 5 show the absorption spectra (Si_{abs}) in the silicon layer, reflectance spectra (R), and particle absorption spectra (P_{abs}) for the front surface embedded TiOx particles and rear surface aluminum particles of radius $R = 70$ nm for different pitches of the arrays: 150 nm (red), 200 nm (green), 250 nm (blue). The reference cell without nanoparticle arrays is shown by the black line. Clearly, for the reference cell, the particle absorption is zero. The particle absorption spectrum is the sum of the absorption on the front and rear particles. The increase in the
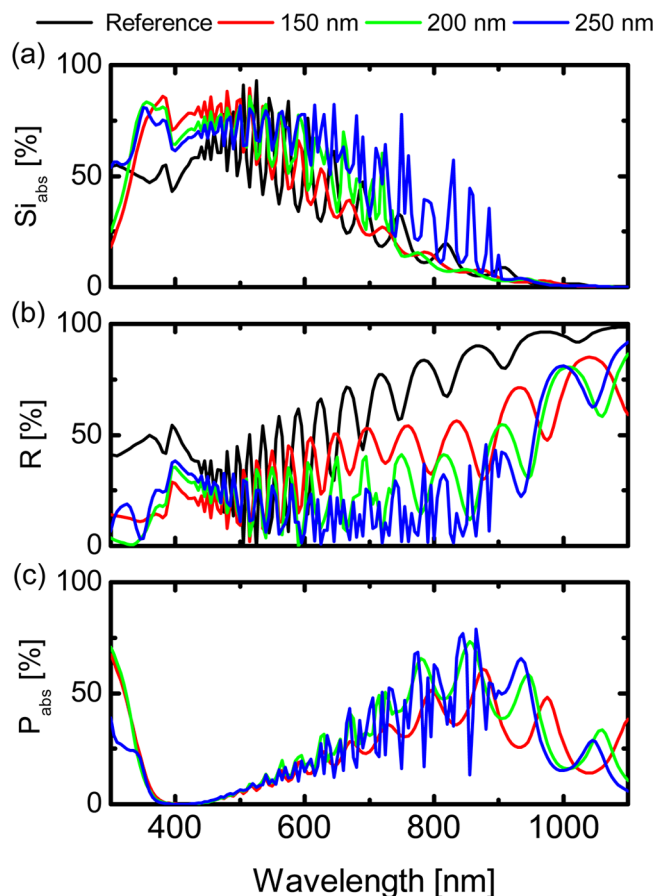

Figure 5. (a) Absorption spectra (Si_{abs}) in the silicon layer, (b) reflectance spectra (R), and (c) particle absorption spectra (P_{abs}) for front surface embedded TiOx particles and rear surface aluminum particles of radius $R = 70$ nm for different pitches of the arrays: 150 nm (red), 200 nm (green), 250 nm (blue). The reference cell without nanoparticle arrays is shown by the black line. The particle absorption spectrum is the sum of the absorption on the front and rear particles. The percentages are calculated from the total incident light intensity.

pitch is shown to increase the strength of the Fabry−Perot resonances due to a better match of the in-plane momentum of the arrays for the range of wavelengths considered. Moreover, the particle absorption does not change significantly with the pitch, in contrast with the reflectance. This clearly demonstrates that the decrease in the reflectance is mostly due to the appearance of diffraction modes at a specific pitch.

Considering the effect of altering the dimension of the nanoparticles, the wavelength-dependent spectra in Figure 6 show the absorption spectra (Si_{abs}) in the silicon layer, reflectance spectra (R), and particle absorption spectra (P_{abs}) for front surface embedded TiOx particles and rear surface aluminum particles of pitch 250 nm for different radii of the particles: 80 nm (black), 70 nm (red), 60 nm (green), 50 nm (blue), 40 nm (cyan). The particle absorption spectrum is the sum of the absorption on the front and rear particles. Smaller aluminum particles on the back surface are shown to cause reduced diffraction and, therefore, higher reflectance and lower absorption, due to their smaller optical cross section. Interestingly, the increase in size of the nanoparticles is shown to red-shift the Fabry−Perot peaks. The red-shift can be simply explained with the increase of the effective refractive
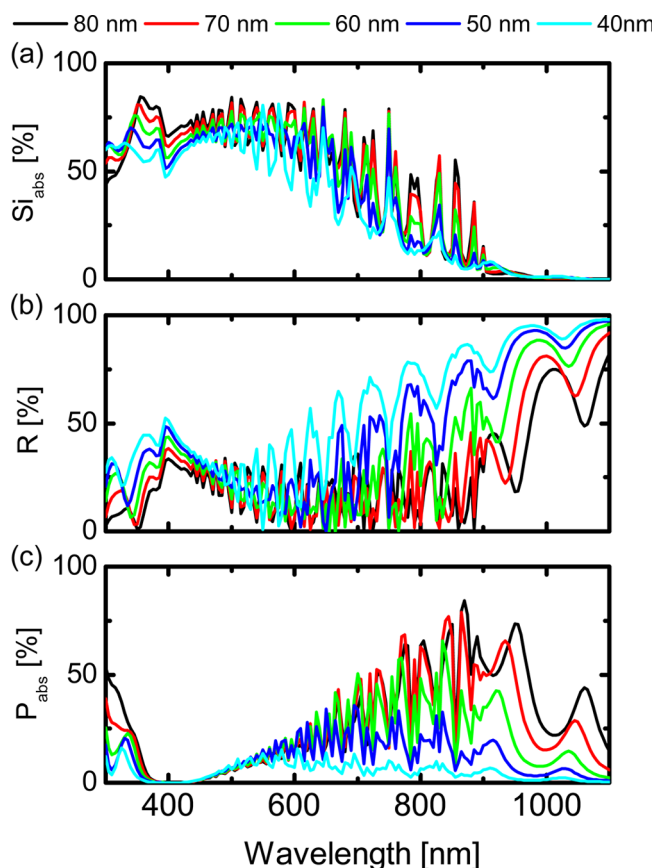
Figure 6. (a) Absorption spectra (Si_{abs}) in the silicon layer, (b) reflectance spectra (R), and (c) particle absorption spectra (P_{abs}) for front surface embedded TiOx particles and rear surface aluminum particles of pitch 250 nm for different radii of the particles: 80 nm (black), 70 nm (red), 60 nm (green), 50 nm (blue), 40 nm (cyan). The particle absorption spectrum is the sum of the absorption on the front and rear particles. The percentages are calculated from the total incident light intensity.

index of the Fabry−Perot cavity when increasing the size of the particles.

Figure 7 shows the absorption spectra (Si_{abs}) in the silicon layer, reflectance spectra (R), and particle absorption spectra (P_{abs}) for front surface embedded particles and rear surface aluminum particles of radius R = 80 nm and pitch 250 nm for different materials of the front surface embedded particles: AlOx (red), SiNx (green), TiOx (blue), Si (cyan). The reference cell without nanoparticle arrays is shown by the black line. The particle absorption spectrum is the sum of the absorption on the front and rear particles. Using embedded silicon nanoparticles is shown to result in the lowest reflectance and the highest absorption in the silicon layer compared to the other dielectrics. It is worth noting that TiOx, AlOx, and SiNx have very small absorption above 400 nm. The reduced reflectance obtained using silicon nanoparticles can be explained by the absence of any optical constant mismatch between the scattering particle and the absorbing layer, being the same material, and by the highest index contrast with the embedding silica layer compared to the other materials.

■ CONCLUSIONS

In summary, a significant photocurrent enhancement in thin-film crystalline silicon solar cells has been obtained due to
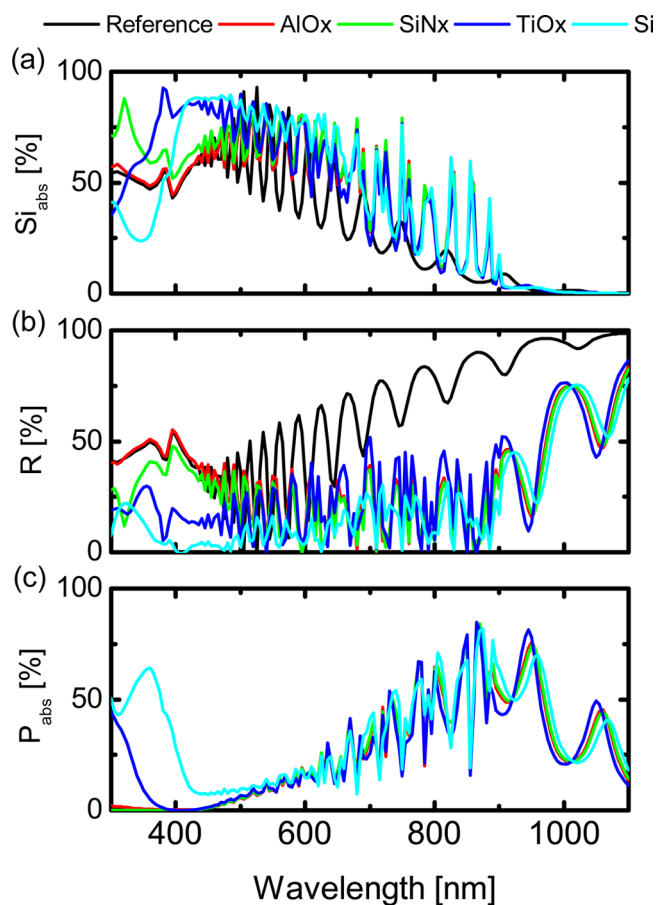

Figure 7. (a) Absorption spectra (Si_{abs}) in the silicon layer, (b) reflectance spectra (R), and (c) particle absorption spectra (P_{abs}) for front surface embedded particles and rear surface aluminum particles of radius R = 80 nm and pitch 250 nm for different materials of the front surface embedded particles: AlOx (red), SiNx (green), TiOx (blue), Si (cyan). The reference cell without nanoparticle arrays is shown by the black line. The particle absorption spectrum is the sum of the absorption on the front and rear particles. The percentages are calculated from the total incident light intensity.

constructive interference arising from diffraction by nano-particle arrays. The mechanism for broad reflectance reduction of the cell by the rear surface array via multiple Fabry−Perot resonances can be described using a simple interference model that considers the effect of the incident and scattered/diffracted light from the particle array. The interference model shows agreement with full field electromagnetic simulations, which involved nanoparticle arrays of metal (aluminum) and dielectrics (silicon, titanium oxide, aluminum oxide, and silicon nitride) of different radius, pitch, and position on the front and rear surface of thin-film crystalline silicon solar cells with antireflection coating, in order to improve light trapping and absorption. We have shown an increase in the estimated short-circuit photocurrent in the absorbing silicon layer over the useful solar spectrum (AM 1.5G) for a 1 μm thick crystalline silicon cell of 46.7% when the nanoparticle arrays are placed on the front and rear surface of the cell with dielectric (Si) particles on the front and metal (Al) particle on the rear surface (J_{sc} = 19.05 mA/cm^2), compared to the cell without nanoparticles (J_{sc} = 12.98 mA/cm^2). An estimated photocurrent enhancement of 29.4% is shown with just the aluminum nanoparticle array on the rear surface of the cell (J_{sc} = 16.80 mA/cm^2). The front

surface array is shown to broadly reduce the reflectance due to the excitation of local resonances and preferential scattering into the substrate. Together with resonance excitation, these two combined effects are significant in general for the design of thin-film solar cells with light-trapping properties to increase the absorption in order to improve cell performance.

■ AUTHOR INFORMATION

Corresponding Author

*E-mail: enrico.massa08@imperial.ac.uk.

Present Address

[⊥]Qatar Environment and Energy Research Institute (QEERI), Qatar Foundation, Doha, Qatar

Notes

The authors declare no competing financial interest.

■ REFERENCES

(1) Shah, A.; Torres, P.; Tscharner, R.; et al. Photovoltaic technology: the case for thin-film solar cells. *Science* **1999**, *285*, 692−698.

(2) Chopra, K.; Das, S. *Thin Film Solar Cells*; Springer, 1983; pp 1−18.

(3) Atwater, H. A.; Polman, A. Plasmonics for improved photovoltaic devices. *Nat. Mater.* **2010**, *9*, 205−213.

(4) Yablonovitch, E.; Cody, G. Intensity enhancement in textured optical sheets for solar cells. *IEEE Trans. Electron Devices* **1982**, *29*, 300−305.

(5) Yablonovitch, E. Statistical ray optics. *J. Opt. Soc. Am.* **1982**, *72*, 899−907.

(6) Trompoukis, C.; El Daif, O.; Depauw, V. et al. Photonic assisted light trapping integrated in ultrathin crystalline silicon solar cells by nanoimprint lithography. *Appl. Phys. Lett.* **2012**, *101*.

(7) Depauw, V.; Meng, X.; El Daif, O.; et al. Micrometer-thin crystalline-silicon solar cells integrating numerically optimized 2-D photonic crystals. *IEEE J. Photovoltaics* **2014**, *4*, 215−223.

(8) Craig, F. Bohren, D. R. H. *Absorption and Scattering of Light by Small Particles*; John Wiley & Sons, 1983.

(9) Maier, S. A. *Plasmonics: Fundamentals and Applications*; Springer, 2007.

(10) Massa, E.; Maier, S. A.; Giannini, V. An analytical approach to light scattering from small cubic and rectangular cuboidal nano-antennas. *New J. Phys.* **2013**, *15*, 063013.

(11) Massa, E.; Roschuk, T.; Maier, S. A.; et al. Discrete-dipole approximation on a rectangular cuboidal point lattice: considering dynamic depolarization. *J. Opt. Soc. Am. A* **2014**, *31*, 135−140.

(12) Knight, M. W.; Sobhani, H.; Nordlander, P.; et al. Photodetection with active optical antennas. *Science* **2011**, *332*, 702−704.

(13) Hägglund, C.; Apell, S. P.; Kasemo, B. Maximized optical absorption in ultrathin films and its application to plasmon-based two-dimensional photovoltaics. *Nano Lett.* **2010**, *10*, 3135−3141.

(14) Temple, T. L.; Bagnall, D. M. Optical properties of gold and aluminium nanoparticles for silicon solar cell applications. *J. Appl. Phys.* **2011**, *109*, 084343.

(15) Mokkapati, S.; Beck, F. J.; Polman, A. et al. Designing periodic arrays of metal nanoparticles for light-trapping applications in solar cells. *Appl. Phys. Lett.* **2009**, *95*, 053115.

(16) Dunbar, R. B.; Pfadler, T.; Schmidt-Mende, L. Highly absorbing solar cells—a survey of plasmonic nanostructures. *Opt. Express* **2012**, *20*, A177−A189.

(17) Hylton, N. P.; Li, X. F.; et al. Loss mitigation in plasmonic solar cells: aluminium nanoparticles for broadband photocurrent enhancements in GaAs photodiodes. *Sci. Rep.* **2013**, *3*, 2874.

(18) Spinelli, P.; Hebbink, M.; de Waele, R.; et al. Optical impedance matching using coupled plasmonic nanoparticle arrays. *Nano Lett.* **2011**, *11*, 1760−1765.

(19) Spinelli, P.; Macco, B.; Verschuuren, M.; et al. Al_2O_3/TiO_2 nano-pattern antireflection coating with ultralow surface recombination. *Appl. Phys. Lett.* **2013**, *102*, 233902−233902−4.

(20) Villesen, T. F.; Uhrenfeldt, C.; Johansen, B. Aluminum nanoparticles for plasmonimproved coupling of light into silicon. *Nanotechnology* **2012**, *23*, 085202.

(21) Beck, F. J.; Mokkapati, S.; Catchpole, K. R. Light trapping with plasmonic particles: beyond the dipole model. *Opt. Express* **2011**, *19*, 25230−25241.

(22) Southwell, W. H. Pyramid-array surface relief structures producing antireflection index matching on optical surfaces. *J. Opt. Soc. Am. A* **1991**, *8*, 549−553.

(23) Parker, A. R.; Townley, H. E. Biomimetics of photonic nanostructures. *Nat. Nanotechnol.* **2007**, *2*, 347−353.

(24) Huang, Y.-F.; Chattopadhyay, S.; Jen, Y.-J.; et al. Improved broadband and quasiomnidirectional anti-reflection properties with biomimetic silicon nanostructures. *Nat. Nanotechnol.* **2007**, *2*, 770−774.

(25) Her, T.-H.; Finlay, R. J.; Wu, C.; et al. Microstructuring of silicon with femtosecond laser pulses. *Appl. Phys. Lett.* **1998**, *73*, 1673−1675.

(26) Branz, H. M.; Yost, V. E.; Ward, S. et al. Nanostructured black silicon and the optical reflectance of graded-density surfaces. *Appl. Phys. Lett.* **2009**, *94*.

(27) Zhu, J.; Yu, Z.; Burkhard, G. F.; et al. Optical absorption enhancement in amorphous silicon nanowire and nanocone arrays. *Nano Lett.* **2009**, *9*, 279−282.

(28) Rivas, J. G.; Vecchi, G.; Giannini, V. Surface plasmon polariton-mediated enhancement of the emission of dye molecules on metallic gratings. *New J. Phys.* **2008**, *10*, 105007.

(29) Santbergen, R.; Tan, H.; Zeman, M.; et al. Enhancing the driving field for plasmonic nanoparticles in thin-film solar cells. *Opt. Express* **2014**, *22*, A1023−A1028.

(30) Catchpole, K. R.; Polman, A. Plasmonic solar cells. *Opt. Express* **2008**, *16*, 21793−21800.

(31) Ferry, V. E.; Munday, J. N.; Atwater, H. A. Design considerations for plasmonic photovoltaics. *Adv. Mater.* **2010**, *22*, 4794−4808.

(32) Li, X.; Hylton, N. P.; Giannini, V.; et al. Multi-dimensional modeling of solar cells with electromagnetic and carrier transport calculations. *Prog. Photovoltaics* **2013**, *21*, 109−120.

(33) Li, X.; Hylton, N. P.; Giannini, V.; et al. Bridging electromagnetic and carrier transport calculations for three-dimensional modeling of plasmonic solar cells. *Opt. Express* **2011**, *19*, A888−A896.

(34) Catchpole, K. R.; Polman, A. Design principles for particle plasmon enhanced solar cells. *Appl. Phys. Lett.* **2008**, *93*, 191113.

(35) Zhang, Y.; Ouyang, Z.; Stokes, N. et al. Low cost and high performance Al nanoparticles for broadband light trapping in Si wafer solar cells. *Appl. Phys. Lett.* **2012**, *100*, 151101.

(36) Akimov, Y.; Koh, W. Design of plasmonic nanoparticles for efficient subwavelength light trapping in thin-film solar cells. *Plasmonics* **2011**, *6*, 155−161.

(37) Uhrenfeldt, C.; Villesen, T.; Johansen, B.; et al. Tuning plasmon resonances for light coupling into silicon: a "rule of thumb" for experimental design. *Plasmonics* **2013**, *8*, 79−84.

(38) Palik, E. D. *Handbook of Optical Constants of Solids*; Academic, 1985.

(39) Giannini, V.; Zhang, Y.; Forcales, M.; et al. Long-range surface polaritons in ultra-thin films of silicon. *Opt. Express* **2008**, *16*, 19674−19685.